Development of an ultrasonic experimental device to characterise concrete for structural repair

Farouk Benmeddour, Géraldine Villain, Odile Abraham, Marta Choinska

Development of an ultrasonic experimental device to characterise concrete for structural repair

Farouk Benmeddour [a,b,*], Géraldine Villain [a], Odile Abraham [a], Marta Choinska [c]

[a] L'Université Nantes Angers Le Mans (L'UNAM), IFSTTAR, MACS, F-44341 Bouguenais, France
[b] IEMN, OAE Department, CNRS UMR 8520, University of Valenciennes and Hainaut Cambrésis, Le Mont Houy, 59313 Valenciennes Cedex 9, France
[c] L'Université Nantes Angers Le Mans (L'UNAM), GeM – Research Institute of Civil Engineering and Mechanics, CNRS UMR 6183, Nantes University – IUT Saint-Nazaire, 58 rue Michel Ange, 44600 Saint-Nazaire, France

Various non destructive testing methods, based on the propagation of ultrasonic waves, can be used to characterise the mechanical properties of structural concrete in situ. The results obtained however are heavily influenced by both water content and concrete mix design. To overcome these biases, it is neces sary to recalibrate the results on a small number of cores, whose water content has been laboratory con trolled. To this end, an experimental device designed around the transmission of bulk waves has been developed. The aim of this paper is to introduce and describe such a device, which is able to take into account specimen size, centre frequency and ease of use. The studied mixes herein are composed of wet shotcrete, dry shotcrete and concrete that has been formed and manually set. Measurement results show the evolution in wave velocities relative to four degrees of saturation. Moreover, measurement uncertainties in the values of velocities, Young's modulus, shear modulus and Poisson's ratio are quantified.

1. Introduction

Various ultrasonic non destructive methods are available for characterising the mechanical properties of concrete cores in the laboratory or in situ reinforced concrete structures [1 11]. The re sults derived from methods introduced in situ however are heavily influenced by water content, concrete mix design and external conditions, as revealed in the French project ANR SENSO [12 14], during which ultrasonic results were correlated with mechanical properties and porosity for concretes under homogeneous mois ture conditions. These empirical relationships could then be used to estimate the in situ porosity thanks to ultrasonic measurement results [15]. It was demonstrated that this estimation is more accu rate for the specific concrete mix chosen to establish the relation ship. Yet each concrete structure was designed with a different concrete mix and then exposed to different environmental condi tions. In order to overcome these formulation and moisture biases, it becomes necessary to recalibrate the results due to ultrasonic wave propagation on a small number of cores whose water content has been accurately controlled in the laboratory.

The in situ measurement techniques tested during the ANR SENSO project are based on measurements of the compression wave velocity in transmission and the surface wave velocity [16], as well as on the impact echo method [15,17] for calculating the compression (P), shear (S) and Rayleigh (R) wave velocities in addition to the dynamic Young's modulus and Poisson's ratio of both beams and slabs. To recalibrate the results yielded by these

* Corresponding author at: IEMN, OAE Department, CNRS UMR 8520, University of Valenciennes and Hainaut Cambrésis, Le Mont Houy, 59313 Valenciennes Cedex 9, France.
E-mail address: Farouk.Benmeddour@univ-valenciennes.fr (F. Benmeddour).

techniques, a determination of the dynamic Young's modulus and Poisson's ratio at various frequencies is critical. To produce such a determination, the compression P and shear S wave velocities at various frequencies need to be recorded. For this purpose, a measurement device based on P and S wave propagation in transmission has been developed as part of the present study.

The objectives of this paper are twofold: first to present the device that meets specific recalibration requirements in terms of specimen dimensions, centre frequency and ease of use; and second to display the initial measurement results on various repair materials differentiated by their water content.

The first part of this paper will be devoted to the description of the experimental device. The set of design constraints imposed on both the device and samples will be described. Choices regarding signal frequency, transducers and supports will be analysed along with the errors generated by dimensioning constraints. Next, a dedicated signal processing software package will be run in order to determine the P and S wave velocities and deduce the dynamic Young's modulus and Poisson's ratio in addition to their uncertainties. The device validation step is performed using standard materials (PolyVinyl Chloride "PVC", PolyTetraFluoroEthylene "PTFE" and aluminium "Al").

The second part of this paper will focus on the experimental results. The four repair materials, test sample preparation and material characterisation will all be presented. Sample preconditioning and the set of ultrasonic testing conditions will be discussed before analysing the experimental results in drawing conclusions with respect to the water content of concrete.

This ultrasonic device has been designed within the framework of the project FUI MAREO (acronym for MAintenance and REpair of marine concrete structures, Optimisation by risk analysis). The objective of this project is to evaluate the performance of various repair materials through the use of both destructive and non destructive testing methods. A total of four repair materials containing cement have thus been studied; these materials differ from one another by either their mix design or corresponding repair technique.

2. Design and validation of the experimental device

2.1. Constraints imposed on the ultrasonic device

It was found in a previous work [14,18] that the establishment of a diagnosis that takes into account the porosity and water content in concrete by using non destructive (ND) techniques needs the following steps. First, combine complementary measurement techniques based on the propagation of electromagnetic and ultrasonic waves as well as electrical current. Second, determining the calibration curves relating the ND observables (electromagnetic permittivity, electrical resistivity, ultrasonic wave velocities or dynamic moduli) with the physical properties (porosity, degrees of saturation ranging from 40% to 100%), as illustrated in Fig. 1. Third, derive these calibration curves for each mix design type given that the ND observables are influenced and biased by the concrete components and in particular by aggregates.

Fig. 1a shows that the dielectric constant is linearly correlated to water content for six different concretes whereas Fig. 1b shows the linear correlation between the dynamic Young's modulus obtained by the impact echo method and the porosity of the same concretes in saturated and dry conditions. The error bars correspond to the standard deviation of the measurements on three samples for porosity and eight slabs for the dynamic modulus meanwhile very small.

The calibration curves can be obtained on cored samples from the investigated structure. The IFSTTAR Laboratory already possesses an electromagnetic coaxial cylindrical cell [19], while an electrical resistivity cell is currently in the production process. In order to complement these devices, it is therefore necessary to design an ultrasonic device. Therefore, the cored specimens can be investigated by all these devices hence their dimensions must be the same (a height (h) of 70 mm and a 75 mm of diameter). Moreover, the ultrasonic methods used in situ within the scope of the ANR SENSO project are: an ultrasonic transmission device with a typical centre frequency of 250 kHz, two experimental devices for propagating surface waves with a frequency range between 50 and 150 kHz and a measurement device for the impact echo method with low frequencies (from a few kHz to approximatively 25 kHz).

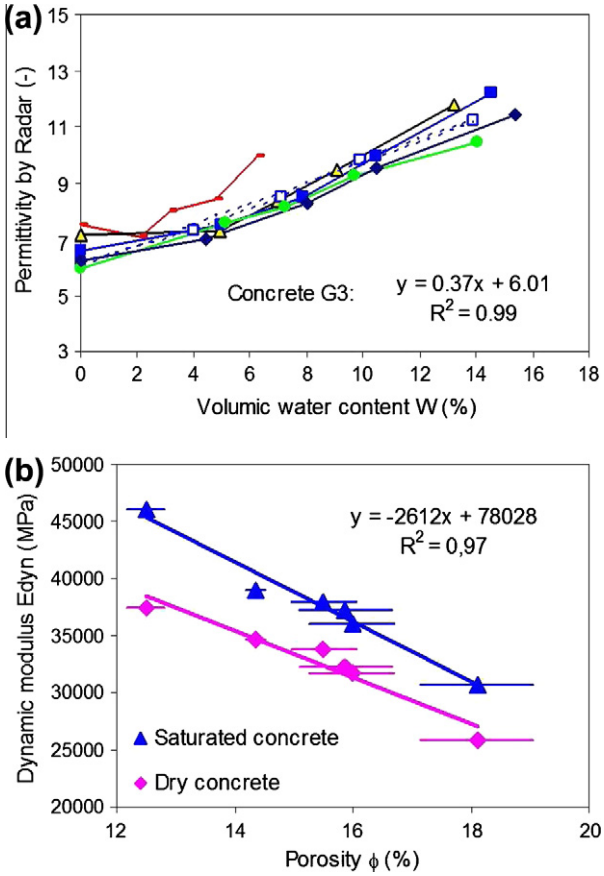

Fig. 1. Example of non-destructive observables correlated with physical properties [14].

It was shown, in the ANR SENSO project, that the linear regression obtained on slabs using these four methods depended on the signal frequency, which thus imposed working at frequencies of less than or equal to 250 kHz.

2.2. Choice and parameterisation of the experimental device

2.2.1. Working frequency

The choice of working frequency (f_c) depends mainly on the wavelength value $\lambda_{P,S} = C_{P,S}/f_c$, where λ denotes the wavelength and subscripts P and S designate the primary and secondary waves, respectively. C_P and C_S represent the respective phase velocities of the compression and shear waves. For the concretes studied herein, the variation ranges of the compression and shear phase velocities examined are [3500 5000 m/s] and [1800 2600 m/s], respectively.

Regarding the imposed small sample size, the choice of centre frequency for the transmitted signal is a compromise that serves

to: avoid the resonance phenomenon by respecting $\lambda/h < 1$, comply to the greatest extent possible with representative volume element (RVE) condition of $\lambda > L_{RVE} > D$, where L_{RVE} and D are the RVE characteristic length and the maximum diameter of the concrete aggregate, respectively and avoid as much as possible any overlap between the emitted and converted waves on the edges of the sample. These conditions require working at a centre frequency of around 250 kHz.

2.2.2. Transducers

The choice of transducers is based on two considerations: first their ability to generate both the compression and shear waves with a good signal to noise ratio, and second their adaptation to hydraulic concrete. Due to boundary conditions and specimen handling time, it is preferable to introduce two transducers (one for P waves the other for S waves) within the same box. To avoid reflections from the edges of cylindrical samples, these transducers must be unidirectional. For this reason, the transduction surface area must be relatively large. The decision was made to use coaxial piezo composite transducers manufactured by the Sonaxis company; these transducers are well adapted to concrete in terms of acoustic impedance and display a very good signal to noise ratio. The compression wave transducer is located at the centre, whereas the shear wave transducer is annular (see Fig. 2). The two piezo composite transducers can be excited independently. Indeed, each generated signal by the P wave emitter is acquired by the P wave receiver and so for the S wave. Then, the measured signals from each transducer are recorded and processed separately from each other.

A coupling gel well suited to shear waves has been applied onto the transducer surfaces to ensure optimal acoustic coupling.

2.3. The experimental device

The measurement protocol requires the production of a support in order to maintain both the samples and transducers. A prototype has been built in the IFSTTAR Laboratory (see Fig. 3). Such a support provides for concentricity of the transducers and sample; moreover, it is adaptable to various specimen sizes.

The emitter is connected to an impulse generator (Sofranel), with the excitation signal being square in shape. The applied voltage amplitude equals 200 V, while the operating frequency is 250 kHz. The receiver is connected to a Sofranel amplifier, whose applied gain can vary between 50 and +50 dB. The received signal is amplified and then sent to an oscilloscope (Fig. 3) for visualisation and averaging. This oscilloscope carries out an averaging over 64 signals. Averaged results are sent to a computer via a GPIB card for both storage and processing.

Signal processing is performed by a dedicated software developed under Matlab. This software offers the ability to modify the time scale in order to facilitate detection of the arrival of either the P or S wave and detect automatically the arrival of the P and S waves by use of one of the two implemented algorithms; correct manually the automatic detection in case of inconsistency and then define a probability range of existence of the S wave arrival due to identification difficulty; determine the dynamic mechanical properties (v, E and G) and associated uncertainties.

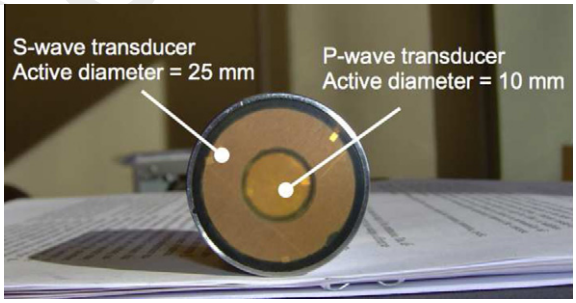

Fig. 2. Sonaxis piezo-composite transducers.

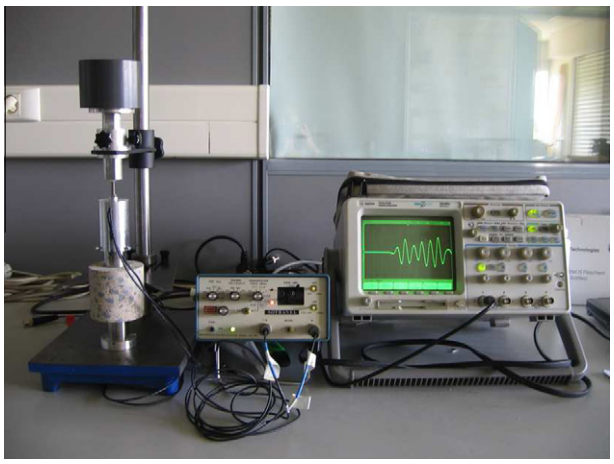

Fig. 3. Close-up of the experimental device.

Two implemented algorithms can detect automatically the arrival of the P and S waves. The first one is based on the detection of a signal perturbation. The second algorithm is based on a sign modification (zero crossing) in a defined time zone. The former is more suitable for the P wave arrival time detection and the latter for the S wave. In fact, when the S wave is easily identified, the suitable automatic algorithm can be used. However, when the latter gives wrong results due to identification difficulty and inconsistency, the user must chose manually the time window in which the probability of the S wave existence is high.

2.4. Experimental protocol and data analysis

The first step of the experimental protocol is the determination of the time of flight between the emitter and the receiver of the P and S waves. This time is subtracted from the measured arrival time since it only depends on the transducers structure and the coupling gel. Studied specimens are weighted then positioned between the transducers in up to down configuration (waves travelling from the top to the bottom of the core). Then, 10 signals are measured and recorded, each of them is the average of 64 signals with a sampling frequency of 40 MHz. Finally, specimens are positioned in down to up configuration (waves travelling from the bottom to the top of the core) and 10 another signals are recorded for treatments.

The arrival time is determined from the acquired signal. The P wave arrival time is easily identifiable due to the high value of the signal to noise ratio (Fig. 4a). However, identification of the S wave arrival time (Fig. 4b) proves difficult, as a result of the presence of either a P wave derived directly from the emitter or a converted S wave at the edges of the cylinder. The fact that P wave velocity exceeds S wave velocity disturbs the identification of S wave arrival time, even though its amplitude remains small. This phenomenon increases uncertainty in the S wave arrival time determination and thus in the shear velocity calculation. The magnitude of the P to S wave ratio depends on the tested material.

In this work, to overcome the detection difficulty mentioned before, the S wave arrival time is determined in a time window range ($[t_{s1}t_{s2}]$). This has the advantage to improve S wave arrival detection but its drawback is the increasing of the uncertainty $\Delta t_S = t_{s2}$

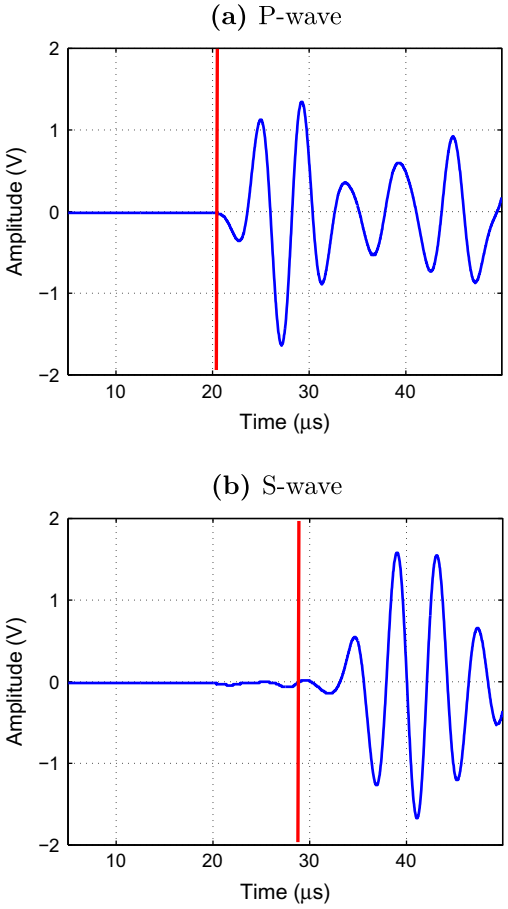

Fig. 4. Time signals of (a) P-wave and (b) S-wave acquired in transmission on a core with $S = 60\%$.

t_{s1}. In future work, it will be necessary to develop more advanced methods for identifying the arrival times of P and S waves.

The height (h) of the cylindrical specimen and its diameter are measured using a calliper at several points so as to obtain the mean values and their corresponding uncertainties (noted Δ), allowing for the calculation of volume and density. The arrival times ($t_{(P,S)}$) and heights are then used to determine the pulse velocities ($C_{(P,S)}$) of P and S waves for each recorded signal. The following results have been recorded from averaging 10 signals for each configuration (i.e. up to down and down to up) as well as for both the P and S waves. The associated uncertainty corresponds to a combination of uncertainty related to the standard deviation of 20 values and uncertainty on the height, as expressed in Eq. (1) below. Moreover, for the S wave, the uncertainty in S wave identification has been taken into account, hence the large error bar magnitudes.

$$C_{(P,S)} \quad \frac{h}{t_{(P,S)}},$$
$$\Delta C_{(P,S)} \quad \sqrt{\left(\left|\frac{1}{t_{(P,S)}}\right|\Delta h\right)^2 + \left(\left|\frac{h}{t^2_{(P,S)}}\right|\Delta t_{(P,S)}\right)^2}. \tag{1}$$

Lastly, the Poisson's ratio (ν), the Young's modulus (E) and the shear modulus (G) and their associated uncertainties are given below:

$$\nu \quad \frac{2C^2_{(T)} \quad C^2_{(L)}}{2(C^2_{(T)} \quad C^2_{(L)})},$$
$$\Delta\nu \quad \sqrt{\left(\left|\frac{C_{(L)}C^2_{(T)}}{(C^2_{(T)} \quad C^2_{(L)})^2}\right|\Delta C_{(L)}\right)^2 + \left(\left|\frac{C_{(T)}C^2_{(L)}}{(C^2_{(T)} \quad C^2_{(L)})^2}\right|\Delta C_{(T)}\right)^2}, \tag{2}$$

$$E \quad \rho C^2_{(L)}\frac{(1+\nu)(1 \quad 2\nu)}{1 \quad \nu},$$
$$\Delta E \quad \left[\left(\left|C^2_{(L)}\frac{(1+\nu)(1 \quad 2\nu)}{1 \quad \nu}\right|\Delta\rho\right)^2 + \left(\left|2\rho C_{(L)}\frac{(1+\nu)(1 \quad 2\nu)}{1 \quad \nu}\right|\Delta C_{(L)}\right)^2 + \left|\rho C^2_{(L)}\frac{2\nu(\nu \quad 2)}{(1 \quad \nu)^2}\right|\Delta\nu\right)^2\Bigg]^{\frac{1}{2}}, \tag{3}$$

$$G \quad 2\rho C^2_{(T)},$$
$$\Delta G \quad \sqrt{\left(|C^2_{(T)}|\Delta\rho\right)^2 + (|2\rho C_{(T)}|\Delta C_{(T)})^2}. \tag{4}$$

3. Experimental procedure

3.1. Repair materials

Three industrial repair concretes have been applied using four different implementation techniques: (I) wet shotcrete, (II) dry shotcrete, (III) manually-implemented concrete, and (IV) formed concrete. The repair concretes (I) and (III) were based on the same mix design. These materials and techniques have been chosen in accordance with European standards [20] and applied in order to repair reinforced concrete beams that had been polluted by chlorides within a tidal zone and then purged by means of hydro-demolition before undergoing repairs in September 2008. As part of this procedure, 10 slabs of each material were cast for testing various destructive and non-destructive characterisation methods [21,22], with an emphasis on the following NDT techniques: impact-echo, surface waves, multi-offset radar, and the capacitive method [23]. Furthermore, it should be noted that after this repair work, all surfaces were levelled in order to improve surface roughness.

Slab number 10, prepared with dimensions of 50 × 50 cm and 25 cm high, was designed for coring. In the following discussion, the study focuses on cored samples extracted from this slab. A cored cylindrical sample with a diameter of 75 mm was extracted at the centre of the slab for each material and each method. This cored sample was then sawn into three individual samples 70 mm high numbered from 1 to 3 depending on the position: 1 for upper (formwork surface), 2 for the middle, and 3 for lower (bottom of the mould). For mix (II), the slab contained cracks and voids; consequently, a second slab of dry shotcrete, labelled IIb was cast and two new samples were cored (i.e. 1 and 3). Each of the 14 samples was identified by a code (like III-2) indicating both the repair technique and sample position.

3.2. Material characterisation

The mechanical characteristics were determined experimentally on cores of dimensions (ϕ95 × 240 mm) derived from slab number 10. Eight cylindrical samples were cored for each material. The protocols adopted for measuring compressive strength Rc (three samples), static Young's modulus E_{stat} (two samples) and Poisson's ratio ν (one sample) are all compliant with current standards [24–26] and recommendations [27].

Regarding durability indicators, the bulk porosity accessible to water ϕ and the saturated density of concretes ρ_{sat} were both determined on remaining samples by means of vacuum water saturation in compliance with AFPC-AFREM [28] recommendations.

Table 1 summarises the studied repair materials and techniques along with their mechanical and physical properties [21].

3.3. Sample pre-conditioning

All 14 core samples were cured under water for 8 months. These samples were then considered to be saturated, i.e. $S = 100\%$, where S represents the degree of saturation. These samples were then dried in an oven for 32 days at a temperature $T = 72° \pm 4$ °C. Afterwards, the specimens were weighed twice within a 24-h interval

Table 1
Properties of the four repair materials and corresponding techniques: (I) wet shotcrete, (II) dry shotcrete, (III) manually implemented concrete and (IV) formed concrete.

Code	R_c (MPa)	E_{stat} (GPa)	ν	ρ_{sat} (kg/m^3)	ϕ (%)
I	54.4 ± 0.5	32.5 ± –	0.27	2274 ± 18	20.6 ± 0.6
II	49.3 ± 0.5	31.8 ± 1.1	0.22	2371 ± 18	12.6 ± 0.3
III	50.0 ± 0.5	23.0 ± 0.1	0.22	2226 ± 12	22.4 ± 1.0
IV	67.1 ± 0.5	34.3 ± 0.2	0.25	2359 ± 16	16.6 ± 0.8

to ensure that they were completely dry and compliant with the criterion recommended in the AFPC-AFREM [28] method:

$$\frac{M_t - M_{t+24h}}{M_t} \leqslant 0.05\%. \quad (5)$$

The samples were considered to be dry ($S = 0\%$) once the above equation had been satisfied.

The next targeted degree of saturation was $S = 30\%$, which could be derived by moistening the samples through imbibition until reaching the desired mass. The specimens were then protected by a plastic wrap and aluminium adhesive foil before being placed in an oven at $T = 62° \pm 4\ °C$ for 3 weeks in order to homogenise water distribution inside the cores, according to the protocol recommended by Parrott [29]. The specimens were again weighed just prior to the ultrasonic measurements, allowing for computation of the real degree of saturation S_r (Table 2).

The second targeted degree of saturation was $S = 60\%$. Both the imbibition and homogenisation phases of moisture rely on the same protocol as for the degree of saturation target $S = 30\%$. The real degrees of saturation calculated just before conducting the ultrasonic measurements are shown in Table 2.

The final targeted degree of saturation was $S = 100\%$. The cored samples were saturated with water under a vacuum, in accordance with the protocol recommended by AFPC-AFREM [28]; next, they were immersed in water for several days before being measured. It should be noted that some samples had not been fully saturated. Consequently, the saturated mass is actually the maximum of the weighing results after curing and after the second saturation under vacuum. The real degree of saturation immediately before the ultrasonic measurements was then calculated.

For all measurements and targeted degrees of saturation $S = 0\%$, 30%, 60% and 100%, the centre operating frequency equals 250 kHz.

4. Characterisation of the repair materials with respect to the water content

In this section, results for the various degrees of saturation are presented in terms of the real degree of saturation calculated by using the mass values. It is worth noting that for the dry state, these measurements have been carried out without either the support of transducers, which ensure the centring of samples relative to transducers, nor the adapted coupling gel for shear waves. These results therefore have not been presented in the paper except for the P wave velocity. Indeed, P wave has a good noise to ratio signal and has the highest velocity.

4.1. Determination of bulk wave velocities

Fig. 5 shows the P wave velocity measurement results of all concrete samples I through IV. Results obtained for the second batch (i.e. II_b) of the dry shotcrete (II) are reported in the series of figures corresponding to this concrete mix. Note that the error bars are small for P waves, thus indicating that the measurements are reproducible on the 10 measurements of each configuration.

The protocol and analysis of results are satisfactory for P waves. The differences between the three specimens of each concrete can be explained by the material variability [30] and position. It can be observed that results on concretes I (wet shotcrete) and III (manual repair), produced with the same material composition, show discrepancies. Sample 1, located near the worked surface, seems to behave differently from samples 2 and 3, which are located in the centre and bottom of the mould, respectively.

Though specimens II and II_b (dry shotcrete) correspond to two different batches of the same mix formulation, the P wave velocity values have the same order of magnitude, yet differences from one batch to the next are clearly visible. For concrete sample IV specimens (formed concrete), results of the P wave velocity values present the same order of magnitude.

For most of the concrete test specimens, we have observed that P wave velocity increases as the degree of saturation rises from 30% to 100%. This can be explained by the greater increase of the sample Young's modulus than the simultaneous increase of density. A slight decrease or nearly constant value of the P wave velocity has been recorded between the nearly dry state and the state corresponding to $S = 30\%$. This phenomenon is more difficult to explain: we tried to explain these results thanks to forces existing in unsaturated media with a very fine micro structure such as concrete. In fact, samples are dried at 70 °C to avoid hydrates degradation thus, they are not fully dried, meanwhile, to be able to calculate the degree of saturation we have assumed that the equilibrium mass reached at 70 °C is the dry mass. The real degree of saturation is near 5%. The lower is the saturation degree, the finer are the pores involved by drying and the higher are the capillary forces [31]. So it could be assumed that the remaining water content contributes to rigidify the porous material therefore induces a higher velocity for the nearly dry state than for $S = 30\%$ [14,17]. This latter has also been observed for soils [32,33].

Fig. 6 depicts the S wave velocity vs. the degree of specimen saturation. This figure reveals a slight velocity increase in the S wave with the degree of saturation, although this trend shows the same order of magnitude as measurement uncertainty. In the future therefore, it will be necessary to reduce uncertainty in order to draw actual conclusions.

4.2. Mechanical moduli

Fig. 7 shows the results of the Poisson's ratio computations. The Poisson's ratio values obtained are on the order of 0.24. This parameter does not change significantly enough to distinguish the various concrete specimens.

Figs. 8 and 9 present the Young's dynamic modulus and the shear dynamic modulus, respectively computed with Eqs. (3) and (4). These moduli increase as the degree of saturation rises from 30% to 100%, with the same trend noticed for velocity and density. It is worth noting that the unexpected results of G and v are due to the difficulty to obtain the shear wave arrival time with a good accuracy. The error bars of G and v are highly influenced by this arrival time.

4.3. Comparison of results obtained by different techniques

In what follows, the obtained results are compared to those obtained by three different methods: the mechanical resonance frequencies (Grindosonic), the mechanical destructive technique and the impact echo.

The commercial device Grindosonic (denoted Grindo) is based on a frequency resonance technique [34 37] by exciting the core with a wood made ball. Two fundamental frequencies are measured to derive the Young's modulus and the Poisson's coefficient. In this study, the Grindosonic tests have been performed on the whole specimen (240 mm high).

The destructive method permit to get static Young's modulus (denoted "stat") which is based on longitudinal displacement of a specimen recorded during application of three loading cycles cor

Table 2
Mass measurements of samples (g) vs. saturation level S (%).

	$S_{r,30\%}$	$S_{r,60\%}$	$S_{r,100\%}$
I-1	28.26	56.89	100.00
I-2	27.80	56.70	99.36
I-3	27.93	55.74	98.25
II-1	24.72	59.51	100.00
II-2	29.12	56.90	100.00
II-3	28.64	56.03	100.00
III-1	28.82	59.30	98.26
III-2	29.20	62.27	99.92
III-3	29.07	58.50	97.16
IV-1	28.19	57.59	100.00
IV-2	28.51	61.34	99.02
IV-3	27.70	51.61	98.05
II_b-1	28.48	53.00	100.00
II_b-3	28.00	55.67	97.28

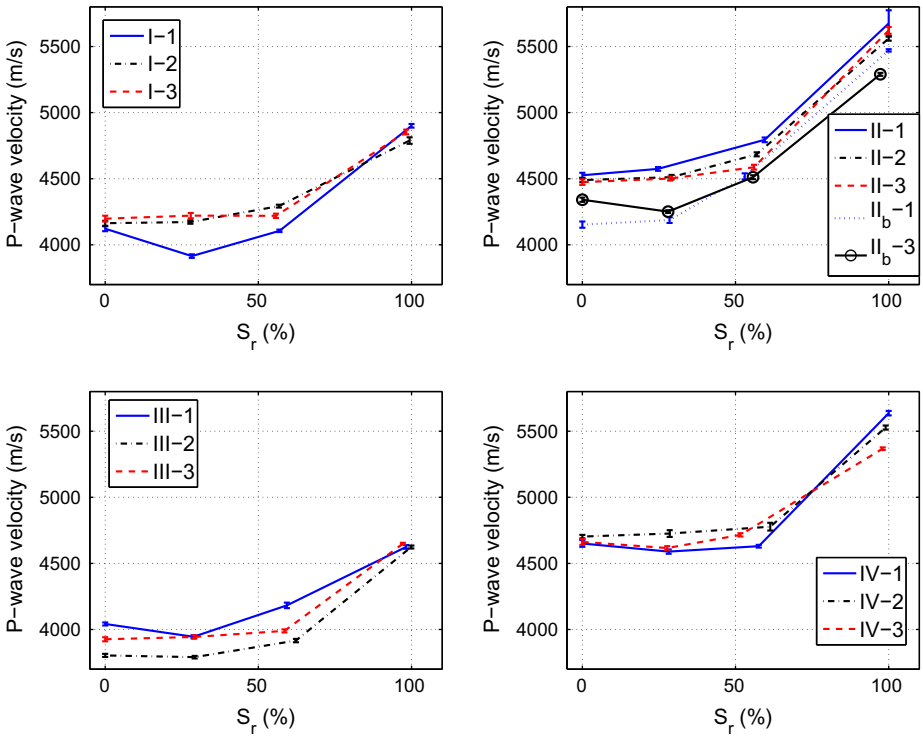

Fig. 5. Compression wave velocities of the various cores.

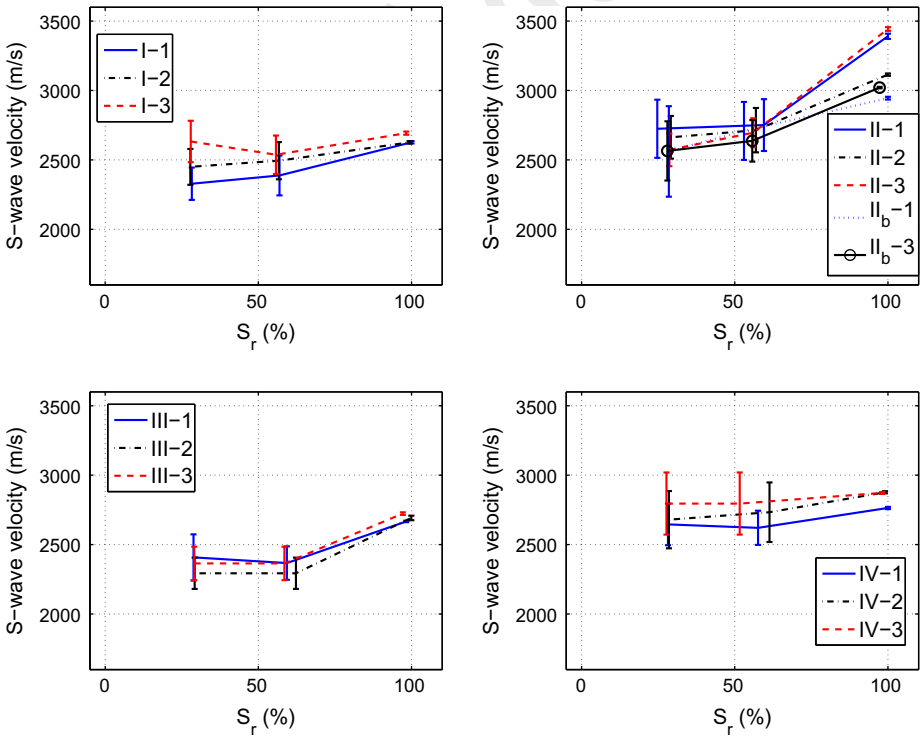

Fig. 6. Shear wave velocities of the various cored samples.

responding to 40% of the compressive strength [26]. Poisson's ratio is obtained when transversal displacement of a specimen is also recorded. Here, the longitudinal displacement measurements have been performed on the central part of a specimen using a cell of 100 mm high. The impact echo method consists in the measurement of resonance frequencies on water saturated slabs. The main characteristic frequency corresponds to the first symmetrical Lamb mode (S_1). For slabs, the other measured frequencies are identified to resonance bending modes. Then, the Young's modulus and the Poisson's coefficient, denoted "dyn IE", are obtained by using an inversion algorithm [15,17]. Results of the afore studied ultrasonic device in transmission mode on cores are denoted "US dyn".

Fig. 10 provides the values of Young's modulus and Poisson's ratio. These Young's moduli are consistent with the saturated density

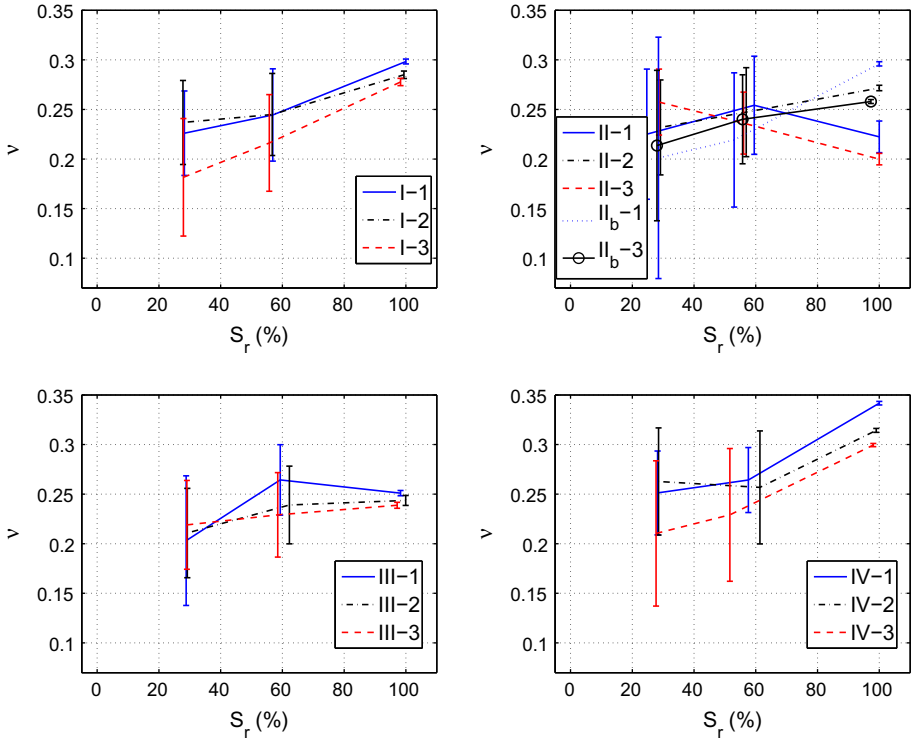

Fig. 7. Poisson's ratio values identified for the various specimens.

and porosity measurements for each of the four materials. As for the dynamic Young's modulus values determined by both the impact echo method and ultrasonic transmission device, they are greater than the static modulus values; moreover, as frequency increases, the modulus value also rises (thereby corroborating the results of the SENSO project). The error bars have been computed for 2 or 3 core or slab specimens.

The measurements are highly scattered when applying either the transmission method or the impact echo method. In statics, measurements may be performed on just a single core; for this reason, the error bar is absent.

The measurements carried out using Grindo produce aberrant Poisson's ratio values. Normally dynamic moduli are greater than static ones, which is not the case for the shotcrete samples. First,

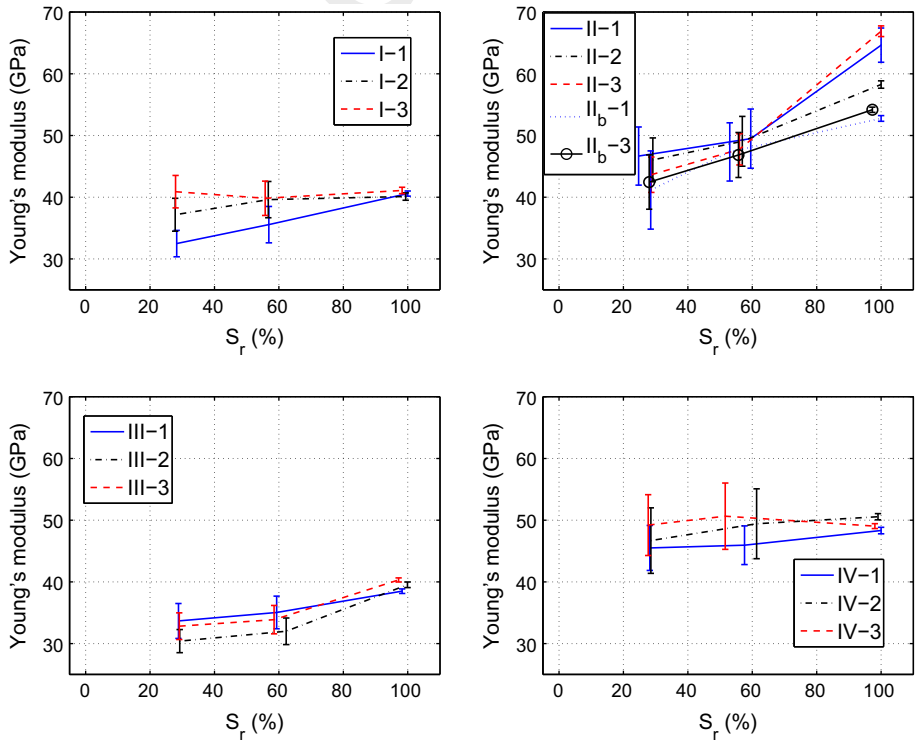

Fig. 8. Young's modulus values derived for various specimens.

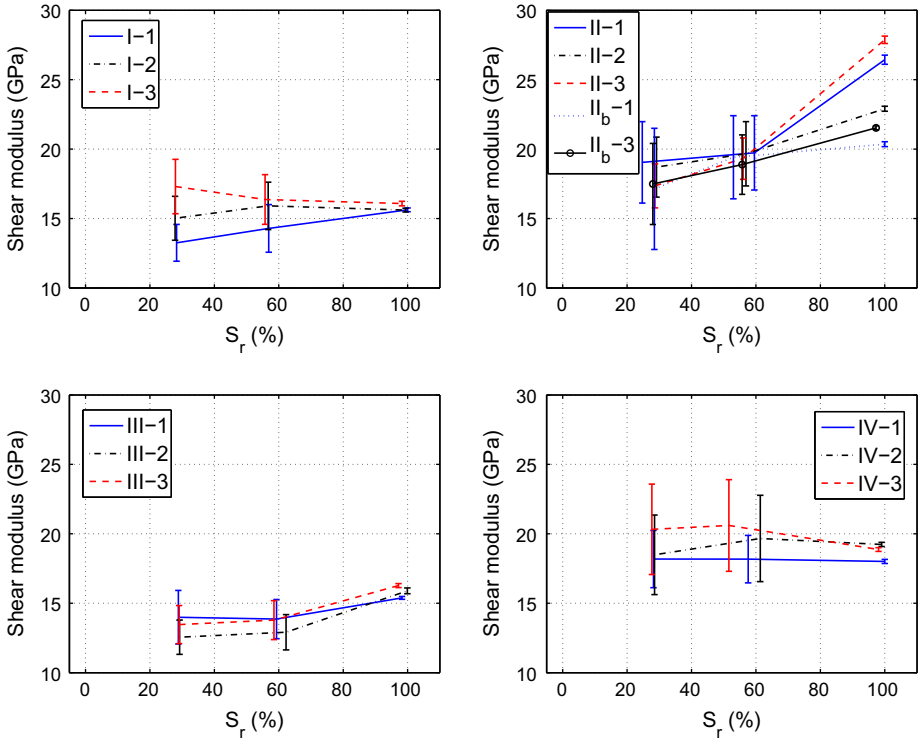

Fig. 9. Shear modulus values derived for various specimens.

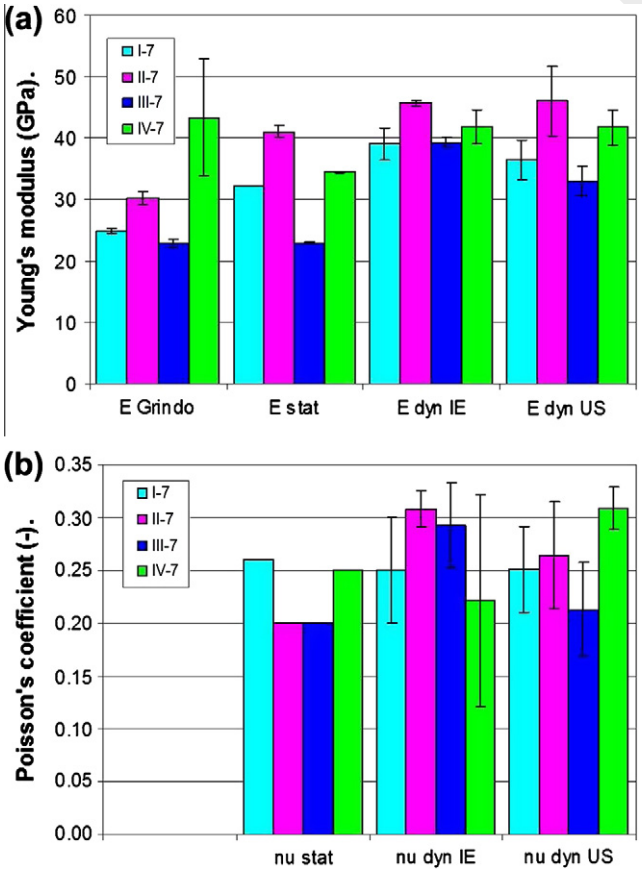

Fig. 10. Comparison of the results obtained from all 4 methods (Grindosonic, under press or static, impact-echo and transmission device) relative to: (a) Young's modulus and (b) Poisson's ratio.

the Grindosonic tests and the static measurements have been carried out on other samples which dimensions are different from those used in this work. After being cored in slabs of 500 mm × 500 mm × 250 mm, their diameter and height were equal to 95 mm and 240 mm, respectively. The Grindosonic tests have been performed on the whole specimen (240 mm high). By the way, the recommended elongation for the Grindo device (twice the diameter) is not respected in this work. Second, the unexpected effect is observed principally for the both shotcretes, I and II, for which the extremities are strongly affected by the casting methods. Indeed, the induced heterogeneities in the hight cause probably the observed decrease in the Grindo moduli in comparison to the static one, because the static measurements have been carried out only on the central part of a specimen using a cell of 100 mm high. Nevertheless, this device being known by the structure inspectors, it was worth to compare it to other ultrasonic methods.

5. Conclusion

In this work, an ultrasonic device in transmission mode has been developed. This device allows characterising cores extracted in situ from a structure. This characterisation process serves to quantify the measurement bias relative to water content. The device consists of two concentric, piezo composite rings that enable generating P and/or S waves at a centre frequency of up to 250 kHz. The centre frequency was chosen so as to satisfy the set of imposed constraints. The transducers and sample supports were designed to ensure centring of the entire assembly. A special contact adapted to S waves has been recommended herein. A dedicated data processing software has also been developed as part of this work programme. The measurement protocol could then be validated on several standard materials.

Four distinct repair materials and techniques were tested during this study. Three cores of each material were pre conditioned in order to obtain homogeneous saturation. All measurements in

the dry state and a few in the saturated state would however need to be repeated. Study results show the evolution in ultrasonic wave velocities and dynamic moduli vs. the degree of saturation. The measurements based on S wave propagation are scattered. Signal arrival is harder to identify given that a P wave is superimposed at the beginning of the wave. The subsequent major uncertainty in S wave velocity measurements influences the calculation of dy namic modulus uncertainties.

The resulting P waves are not scattered. P wave velocity and the dynamic Young's modulus vs. saturation level both increase when the degree of saturation lies between 30% and 100%.

In conclusion, an ultrasonic device is now available to deter mine the regression curve correlating the non destructive results with the degree of saturation, as defined during the ANR SENSO project. This recalibration curve is essential in establishing a dura bility diagnosis of the concrete structure. To deduce simulta neously water content and physical properties (porosity or strength), electromagnetic and ultrasonic results are combined either by multi linear cross correlations or data fusion as de scribed in [15] in particular.

During future research efforts, it will be necessary to verify that the measurements performed on slabs and cores lead to the same recalibration curves. Moreover, a parametric study on the signal centre frequency must be carried out to account for its influence on the dynamic modulus.

Acknowledgements

This work programme has been financed by the French region "Pays de la Loire" (the FUI MAREO Project). The authors are grate ful to O. Coffec, A. Luczak and O. Durand for their valuable experi mental contributions. Their gratitude is also extended to C. Bezias, F. Blaineau and L. M. Cottineau for their assistance during the ultrasonic device development phase.

References

[1] McCann DM, Forde MC. Review of NDT methods in the assessment of concrete and masonry structures. NDT & E Int 2001;34:71–84.
[2] Aggelis D, Hadjiyiangou S, Chai H, Momoki S, Shiotani T. Longitudinal waves for evaluation of large concrete blocks after repair. NDT & E Int 2011;44:61–6.
[3] Shiotani T, Momoki S, Chai H, Aggelis D. Elastic wave validation of large concrete structures repaired by means of cement grouting. Constr Build Mater 2009;23:2647–52.
[4] Rivard P, Saint-Pierre F. Assessing alkali-silica reaction damage to concrete with non-destructive methods: from the lab to the field. Constr Build Mater 2009;23:902–9.
[5] De Belie N, Grosse C, Kurz J, Reinhardt H-W. Ultrasound monitoring of the influence of different accelerating admixtures and cement types for shotcrete on setting and hardening behaviour. Cement Concrete Res 2005;35:2087–94.
[6] Carino N. Nondestructive test methods to evaluate concrete structures. In: Sixth CANMET/ACI international conference on durability of concrete, Thessaloniki, Greece.
[7] Breysse D, Abraham O. Méthodologie d'évaluation non destructive de l'état d'altération des ouvrages en béton. Methodology for non-destructive evaluation of the deterioration state of concrete structures. In: Presses des Ponts et Chaussées, Paris, groupe de travail piloté par D. Breysse et O. Abraham. a.
[8] Vergara L, Miralles R, Gosálbez J, Juanes F, Ullate L, Anaya J, et al. NDE ultrasonic methods to characterise the porosity of mortar. NDT & E Int 2001;34(8):557–62.
[9] Hernández M, Izquierdo M, Ibáñez A, Anaya J, Ullate L. Porosity estimation of concrete by ultrasonic NDE. Ultrasonics 2000;38:531–3.
[10] Bungey J, Millard S. Testing of concrete structures. 3rd ed. Glasgow: Blackie Academic & Professional; 1996.
[11] Cabrera J, Al-Hasan A. Performance properties of concrete repair materials. Constr Build Mater 1997;11:283–90.
[12] Balayssac J-P, Laurens S, Arliguie G, Ploix M, Breysse D, Piwakowski B, et al. évaluation de l'état des ouvrages en béton par combinaison de techniques non destructives. Assessment of the concrete state of structures by combination of non-destructive techniques. In: Actes des journées COFREND, Toulouse, France.
[13] Balayssac J-P, Laurens S, Arliguie G, Ploix M, Breysse D, Piwakowski B, et al. SENSO, a French project for the evaluation of concrete structures condition by combining non destructive testing methods. In: NDTCE'09, Nantes, France. p. 252–391.
[14] Villain G, Dérobert X, Abraham O, Coffec O, Durand O, Laguerre L, et al. Use of ultrasonic and electromagnetic NDT to evaluate durability monitoring parameters of concretes. In: NDTCE'09, Nantes, France. p. 343–8.
[15] Villain G, Sbartaï ZM, Dérobert X, Garnier V, Balayssac J-P. Durability diagnosis of a concrete structure in a tidal zone by combining NDT methods: laboratory tests and case study. Constr Build Mater, in press. http://dx.doi.org/10.1016/j.conbuildmat.2012.03.014.
[16] Abraham O, Piwakowski B, Villain G, Durand O. Non contact ultrasonic measurement for the mechanical characterisation of concrete with surface waves. Constr Build Mater, in press. http://dx.doi.org/10.1016/j.conbuildmat.2012.03.015.
[17] Villain G, Le Marrec L, Rakotomanana L. Determination of the bulk elastic moduli of various concretes by resonance frequency analysis of slabs submitted to impact echo. Eur J Environ Civil Eng 2011;15(4):601–17.
[18] Balayssac J-P, Laurens S, Arliguie G, Breysse D, Garnier V, Dérobert X, et al. Description of the general outlines of the French project SENSO – quality assessment and limits of different NDT methods. Constr Build Mater 2012;35:131–8.
[19] Adous M, Queffelec P, Laguerre L. Coaxial/cylindrical transition line for broadband permittivity measurement of civil engineering materials. Meas Sci Technol 2006;17:2241–6.
[20] NF EN 1504 (1-10), Produits et systèmes pour la protection et la réparation des structures en béton. définitions, prescriptions, maîtrise de la qualité et évaluation de la conformité (Products and systems for the protection and repair of concrete structures: definitions, requirements, quality control and conformity assessment), 2006.
[21] Perrin P, Choinska M, Bonnet S, Boukhouna A, Gaillet L. Repair materials durability of structures in marine environment. In: 2nd conference on marine environment damage to coastal and historical structures, MEDACHS, La Rochelle, France.
[22] Benmeddour F, Villain G, Dérobert X, Abraham O, Schoefs F, Perrin M, et al. Statistical analysis of NDT results for analysing the efficiency of repair techniques of wharves: the MAREO project. In: 11th International conference on applications of statistics and probability in civil engineering, ETH Zurich, Switzerland.
[23] Benmeddour F, Villain G, Schoefs F, Perrin M, Dérobert X, Bonnet S, et al. Combining NDT tools for analysing the efficiency of repair techniques of wharves: the MAREO project. In: Proceedings of the international conference on structural fault and repair, SFR2010, Edinburgh, United Kingdom.
[24] NF EN 206-1. Concrete – Part 1: Specification, performance, production and conformity, 2004.
[25] NF EN 13412. Products and systems for the protection and repair of concrete structures – test methods – determination of modulus of elasticity in compression, 2006.
[26] ASTM C469-02. Standard test method for static modulus of elasticity and Poisson's ratio of concrete in compression, 2010.
[27] Torrenti J, Dantec P, Boulay C, Semblat J-F. Projet de processus d'essai pour la détermination du module de déformation longitudinale du béton (Proposed testing process to determine the longitudinal modulus of concrete deformation). Bulletin des Laboratoires des Ponts et Chaussées 1999;220:79–81.
[28] AFPC-AFREM. Méthodes recommandées pour la mesure des grandeurs associées à la durabilité (Recommended methods for measurement of quantities associated to sustainability), 1997.
[29] Parrott L. Moisture conditioning and transport properties of concrete test specimens. Mater Struct 1994;27:460–8.
[30] Sbartaï Z-M, Breysse D, Larget M, Balayssac J-P. Combining NDT techniques for improved evaluation of concrete properties. Cement Concrete Compos 2012;34:725–33.
[31] Baroghel-Bouny V. Water vapour sorption experiments on hardened cementitious materials. Part I: Essential tool for analysis of hygral behaviour and its relation to pore structure. Cement Concrete Res 2007;37:414–37.
[32] Homand F, Duffaut P. Handbook of rock mechanics, vol. 1. Foundations Manuel de mécanique des roches, Tome 1, Fondements., Comité français de mécanique des roches, 2000.
[33] Murphy WM. Effects of partial water saturation on attenuation in Massilon sandstone and Vycor porous glass. J Acoust Soc Am 1982;71(6):1458–68.
[34] NF 18-414. Essai des bétons, essais non destructifs, mesure de la fréquence de résonance fondamentale (Testing of concrete, nondestructive testing, measurement of fundamental resonant frequency), 1993.
[35] Christaras B, Auger F, Mosse E. Determination of the moduli of elasticity of rocks. comparison of the ultrasonic velocity and mechanical resonance frequency methods with direct static methods. Mater Struct 1994;27:222–8.
[36] Picandet V, Khelidj A, Bastian G. Effect of axial compressive damage on gas permeability of ordinary and high-performance concrete. Cement Concrete Res 2001;31:1525–32.
[37] Schmidt R, Alpern P, Tilgner R. Measurement of the Young's modulus of moulding compounds at elevated temperatures with a resonance method. Polym Test 2005;24:137–43.